OL 98-004

Reprinted from

PHYSICS LETTERS A

Physics Letters A 242 (1998) 51–62

Turbulent diffusion of instantaneous clouds in the atmospheric surface layer: measurements and comparison with Lagrangian similarity theory

Eugene Yee

Defence Research Establishment Suffield, P.O. Box 4000, Medicine Hat, Alberta, Canada T1A 8K6

Received 18 September 1997; revised manuscript received 25 February 1998; accepted for publication 25 February 1998
Communicated by C.R. Doering

ELSEVIER

18 May 1998

PHYSICS LETTERS A

ELSEVIER

Physics Letters A 242 (1998) 51–62

Turbulent diffusion of instantaneous clouds in the atmospheric surface layer: measurements and comparison with Lagrangian similarity theory

Eugene Yee

Defence Research Establishment Suffield, P.O. Box 4000, Medicine Hat, Alberta, Canada T1A 8K6

Received 18 September 1997; revised manuscript received 25 February 1998; accepted for publication 25 February 1998
Communicated by C.R. Doering

Abstract

The structure in a dispersing cloud, obtained from the sudden release of contaminant into the atmospheric surface layer, is experimentally investigated. An adequate number of controlled repeat releases (realizations) has been performed for each set of atmospheric conditions to allow ensemble averages of various functions of the cloud concentration to be obtained. The normalized ensemble-mean concentration and concentration variance crosswind profiles were found to exhibit a self-similar Gaussian form. The evolution of the normalized lateral cloud width and of the normalized cloud centroid ensemble-mean concentration and concentration variance with travel time from the source is investigated. The results of the statistical analysis are compared to predictions of puff dispersion in the constant stress layer obtained from Lagrangian similarity theory. Finally, an examination of the transport equation for the concentration variance shows that the rate of decay of the ensemble-mean concentration and root-mean-square concentration is equal in the turbulent-convective regime of cloud development, which in turn implies that the fluctuation intensity (i.e. standard deviation of concentration divided by mean concentration) remains constant within this regime of development. © 1998 Published by Elsevier Science B.V.

Although there are a number of experimental papers concerning the structure and development of dispersing plumes in the atmosphere released from continuously emitting sources [1–10], there has been relatively little experimental effort expended on the related problem of the structure and development of dispersing clouds (puffs) in the atmosphere resulting from instantaneous or near-instantaneous releases. The dearth of data on the detailed structure of dispersing clouds of pollutant in the atmosphere persists in spite of the fact that instantaneous releases are more realistic for accident assessment than are continuous releases (e.g., catastrophic loss of containment of a toxic industrial gas from a process vessel, storage tank, or pipeline; explosive release of a chemical warfare agent from a bomb or artillery shell, etc.). The relative lack of attention accorded to the experimental study of instantaneous clouds dispersing in the atmosphere as compared to that in continuous plumes arises primarily from the difficulty in the generation and measurement of instantaneous clouds. An instantaneous cloud dispersing in a stationary atmosphere is an intrinsically time-dependent and non-homogeneous phenomenon, requiring the measurement of a large number of re-

0375-9601/98/$19.00 © 1998 Published by Elsevier Science B.V. All rights reserved.
PII S0375-9601(98)00171-6

alizations (replications) of the dispersing cloud under the constraint that conditions at release and in the atmosphere remain unchanged in each realization of the ensemble. However, the intrinsic difficulties in compiling concentration statistics for an instantaneous cloud from a number of realizations of puff dispersion are compounded in atmospheric flows which generally tend to be nonstationary when observed over any extended period of time.

In spite of these difficulties, a small number of experimental investigations of the turbulent diffusion of instantaneous clouds in the atmosphere have been conducted [11–14]. However, none of these experiments involved the controlled repeat releases of an adequate number of instantaneous clouds to permit meaningful ensemble averages of various concentration statistics for the contaminant cloud to be compiled. In many of these investigations, the concentration measured in an individual trial corresponding to the single instantaneous release of a cloud is assumed to be representative of the ensemble-mean concentration, and these observations are then compared directly to atmospheric diffusion models which can be considered as ensemble mean value predictors only. Furthermore, a single realization of a particular cloud release does not enable the statistics of concentration fluctuations in the dispersing cloud to be determined. In view of these problems, we have conducted a series of tracer experiments studying the structure and development of instantaneous clouds dispersing in the atmospheric surface layer. These experiments have addressed basic requirements not met by previous field experiments involving instantaneously released clouds in the atmosphere; namely, the experiments provided repeat realizations of instantaneously released clouds measured with very high-resolution concentration detectors, accompanied by the simultaneous acquisition of high-quality meteorological and turbulence measurements. The focus of this Letter is to describe some preliminary results from these full-scale cloud dispersion experiments, and to compare these results with simple Lagrangian similarity predictions of cloud dispersion. We begin with brief descriptions of the experiment and of the dataset used in this study.

The experimental site is a uniformly homogeneous, hydraulically smooth, and extremely flat area in the middle of the Salt Flats Causeway Site on US Army Dugway Proving Ground in northwestern Utah (40° 08′ 22″ N and 113° 26′ 05″ W). The site is a barren lake bottom consisting of a mixed clay, mud, and salt soil content that forms a very thin salt-laden crust over the naturally high water table. The average roughness length, z_0, of the site is estimated to be about 0.1 mm.

In each trial or experiment, a quantity Q of propylene gas (C_3H_6) was released nearly instantaneously into the atmosphere from a specially designed puff dissemination system, which consisted of an Air Blaster Model ABS-4-2 air cannon with electrically activated controls. The air cannon consisted of a cylinder of pressurized propylene, a quick-acting poppet valve, a solenoid fill-and-release control valve, a high-volume exhaust valve, and a circular deflector plate that was used to regulate the height of the puff release. A computer-controlled gas release system was incorporated with the air cannon to enable the system to operate in a periodic cycle consisting of an on- and off-time (release and separation time, respectively) for the gas release. This feature provided the disseminator with a pulsed mode of operation which was used to repeat trials a number of times under a given atmospheric condition to form a statistical ensemble of puff dispersion realizations.

The propylene puffs were released at a height, z_s, of 1.3 m (height of the center of the initial source puff) and measured by concentration detectors at a height, z_d, of 1.6 m. The 48 detectors that were available for each experiment were arranged in a straight line roughly perpendicular to the mean wind direction with a crosswind extent of 282, 376, or 470 m (which correspond, respectively, to a 6-, 8-, or 10-m spacing between detectors). The sampling line was oriented in the east-west direction to take advantage of the typical northerly winds presiding at the site. Wind speed and direction measured by a propeller-vane anemometer positioned near the source were closely monitored, and when favorable conditions seemed imminent (e.g., the mean wind direction was approximately perpendicular to the sampling line of detectors), a puff was discharged from the air cannon, the samplers began data acquisition, and a trial of an instantaneous release of a cloud was recorded at the sampling line. This trial was repeated n times to provide the puff dispersion realizations required for the construction of a statistical ensemble. The cloud concentrations were measured with fast-response photoionization detectors manufactured commerically by S. & J. Engineering, Inc. (Richmond

102-02550/

Table 1
Summary of principal variables for the statistical ensembles of puff realization. Here, x is the downwind distance (i.e. distance from the source location to the geometric center of the horizontal sampling line); Q is the average mass of material released in each concentration puff; and, n is the number of puff realizations assigned to the ensemble

Ensemble	x (m)	Q (kg)	n
R01	192	0.37	20
R02	192	0.36	11
R03	192	0.36	29
R04	299	0.36	24
R05	354	0.73	18
R06	354	0.73	17
R07	354	0.73	19
R08	354	0.74	31
R09	354	0.75	31
R10	800	0.74	12
R11	800	1.42	31
R12	800	1.33	20
R13	800	1.35	35
R14	800	1.34	22
R15	800	1.33	12
R16	1200	2.35	22
R17	1200	1.80	19

Table 2
Summary of mean meteorological and turbulence conditions measured with a 3-axis sonic anemometer at 2 m. Here U is mean wind speed; σ_u, σ_v, and σ_w are the standard deviations of velocity fluctuations in the alongwind, crosswind, and vertical directions, respectively; u_* is the friction velocity; and, L is the Monin–Obukhov length

Ens.	U (ms^{-1})	σ_u (ms^{-1})	σ_v (ms^{-1})	σ_w (ms^{-1})	u_* (ms^{-1})	L (m)
R01	5.85	0.777	0.842	0.296	0.261	−18.1
R02	5.58	0.683	0.746	0.276	0.262	−36.4
R03	4.60	0.593	0.545	0.231	0.201	−78.6
R04	3.61	0.462	0.429	0.193	0.163	−20.4
R05	3.61	0.657	0.827	0.277	0.203	−4.42
R06	1.98	0.661	0.691	0.241	0.084	−0.4
R07	3.19	0.615	0.651	0.229	0.150	−3.26
R08	4.40	0.566	0.543	0.223	0.190	−17.6
R09	4.61	0.495	0.301	0.225	0.194	−207
R10	3.41	0.371	0.253	0.184	0.160	226
R11	7.38	0.886	0.692	0.360	0.342	−72.3
R12	6.87	0.953	0.865	0.117	0.303	−24.5
R13	4.54	0.801	0.755	0.258	0.214	−10.6
R14	3.69	0.489	0.427	0.198	0.177	−34.0
R15	2.65	0.315	0.211	0.136	0.110	74.3
R16	7.06	1.04	0.929	0.359	0.320	−20.6
R17	5.11	0.615	0.375	0.272	0.246	133

Hill, Ontario, Canada). This detector has a response time of about 0.02 s. The concentration time series corresponding to the puff-cloud passages through the sampling line were digitized with an 18-bit analog-to-digital (A/D) converter at a digitizing frequency of 50 Hz.

In addition to the concentration measurements, micrometeorological data were also collected during the field experiments. The horizonal (u, v) and vertical (w) components of the instantaneous wind velocity were measured with two- and three-axis sonic anemometers/thermometers (models RSWS-201/2A and RSWS-201/3A, Applied Technologies, Inc.) mounted on two 9-m meteorological masts at various levels between 1 and 8 m above the surface. Three-axis sonic anemometers/thermometers were installed at the 2- and 8-m levels and two-axis sonic anemometers/thermometers were placed at the 0.5-, 1-, and 4-m levels on each of the two meteorological masts. The sonic anemometer data, sampled at 10 Hz, were used to characterize the mean wind profile and turbulence characteristics in the surface layer between 1 and 8 m above ground level. Finally, radiosonde, tethersonde, and pilot balloon (pibal) soundings were made during the trials and used to provide wind and temperature profiles throughout the depth of the atmospheric boundary-layer.

The field campaign resulted in 362 individual trials which were stratified in terms of downwind distance and atmospheric conditions to form 17 statistical ensembles of puff realizations for subsequent processing. Pertinent tracer release parameters for each of the 17 ensembles are summarized in Table 1. Table 2 lists the meteorological variables and turbulence statistics that are key to applying surface-layer similarity scaling to the 17 ensembles. The primary effects of the near surface atmospheric flow on the cloud dispersion can be examined in terms of the friction velocity, u_*, and the scaling length for surface-layer turbulence, the Monin–Obukhov length L. Here, the wind velocity components were calculated in a coordinate system with alongwind (x), crosswind (y), and vertical (z) components denoted u, v, and w, respectively. The Monin–Obukhov length was estimated by

$$L = -\frac{\rho c_p u_*^3 T_s}{\kappa g H}, \qquad (1)$$

where ρ is the density of air, c_p is the specific heat of air at constant pressure, κ is von Karman's constant (≈ 0.4), g is the acceleration due to gravity, T_s is absolute temperature, and $H \equiv \rho c_p \overline{w'T'_s}$ is the sensible heat flux. A primed quantity is used to indicate a turbulent fluctuation (departure from the mean value) and the overline $\overline{(\cdot)}$ refers to a time average. The influence of latent heat flux and water vapor density fluctuations was found to be negligible in our field trials and, hence, was not included in the calculation of L. The friction velocity was determined from

$$u_* = [(\overline{u'w'})^2 + (\overline{v'w'})^2]^{1/4}. \qquad (2)$$

Notice from Table 2 that the ensembles of puff realizations were measured under moderately unstable to slightly stable meteorological conditions, with near-constant turbulence conditions.

For the purpose of this study, the data were processed as follows. Firstly, the position of the instantaneous centroid of each puff in an ensemble was determined. To that end, for each puff-cloud passage across the sampling line at a fixed downwind fetch x, digitized records of the instantaneous concentration-time profiles, $\chi^{(j)}(y,t)$ $(j = 1,2,\ldots,n)$, are available as a function of y (lateral distance measured along the crosswind sampling line from some fixed, but otherwise arbitrary origin) and t (travel time measured from the instant of release of the quantity of contaminant). The number of realizations n available varies from ensemble to ensemble (cf. Table 1). For the jth member of a particular ensemble, the centroid of the instantaneous puff in the (y,t) plane at the detector height, z_d, is determined from

$$y_C^{(j)} \equiv \frac{\int\int y\chi^{(j)}(y,t)\,dy\,dt}{\int\int \chi^{(j)}(y,t)\,dy\,dt} \qquad (3)$$

and

$$t_C^{(j)} \equiv \frac{\int\int t\chi^{(j)}(y,t)\,dy\,dt}{\int\int \chi^{(j)}(y,t)\,dy\,dt}. \qquad (4)$$

Hence, $(y_C^{(j)}, t_C^{(j)})$ is the position of the instantaneous centroid of the jth puff realization in a particular statistical ensemble, and this centroid position will vary from realization to realization.

Next, the evaluation of the ensemble averages of various functions of the puff concentration is undertaken after all the realizations $\chi^{(j)}(y,t)$ in the ensemble are translated so that their centroids in the (y,t) plane are made coincident. To this purpose, define

$$y_r \equiv y - y_C^{(j)} \qquad (5)$$

and

$$t_r \equiv t - t_C^{(j)}, \qquad (6)$$

and translate and dilate (or contract) the jth puff concentration realization to give

$$\chi_r^{(j)}(y_r,t_r) = \chi^{(j)}\left(y_r + y_C^{(j)}, (t_r + t_C^{(j)})\frac{U_T^{(j)}}{U_T}\right), \qquad (7)$$

where U_T is the global mean transport speed for all the puff realizations in the ensemble and $U_T^{(j)}$ is the local mean transport speed for the jth realization. Hence, $U_T = n^{-1}\sum_{j=1}^{n} U_T^{(j)}$. The local transport speed $U_T^{(j)}$ for the jth puff realization is determined as follows. For the jth puff, denote by $r^{(j)}$ the Euclidean distance between the source location and the location of the puff centroid $y_C^{(j)}$ along the crosswind sampling line at a fixed downwind fetch x (viz., each statistical ensemble corresponds to puff realizations measured at a fixed downwind fetch under a particular set of constant (approximately or better) meteorological conditions). The local transport speed is calculated as $U_T^{(j)} = r^{(j)}/t_C^{(j)}$, where $t_C^{(j)}$ is defined in Eq. (4). Because the instantaneous wind direction in which a particular puff realization of an ensemble is imbedded is not controllable and predictable, the local transport speed $U_T^{(j)}$ will vary from realization to realization even within the same ensemble. The contraction or dilation (by the factor $U_T^{(j)}/U_T$ (cf. Eq. (7))) in the t-coordinate of the jth puff in an ensemble is used to remove the effects arising from the small difference between the jth local transport speed and the global mean transport speed used to characterize the ensemble.

Once the centroids of the individual puff realizations in a particular statistical ensemble are made coincident, the ensemble means of functions of χ_r can be determined in the normal way (e.g., as an arithmetical average of the function of χ_r). Because the

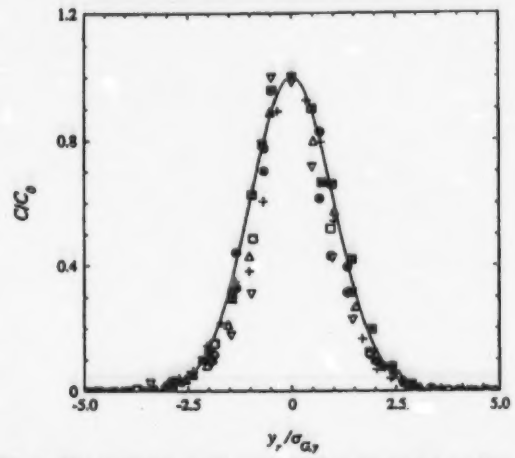

Fig. 1. The ensemble-mean concentration crosswind profiles for the cloud measured in various statistical ensembles at time $t_r = 0$. The ensemble-mean concentration, C, has been normalized by the ensemble-mean concentration, C_0, at the centroid ($C_0 \equiv C(y_r = 0, t_r = 0)$). The lateral profiles are plotted with respect to the normalized crosswind distance, $y_r/\sigma_{G,y}$. The solid line, which plots a standard Gaussian distribution, is included for comparison.

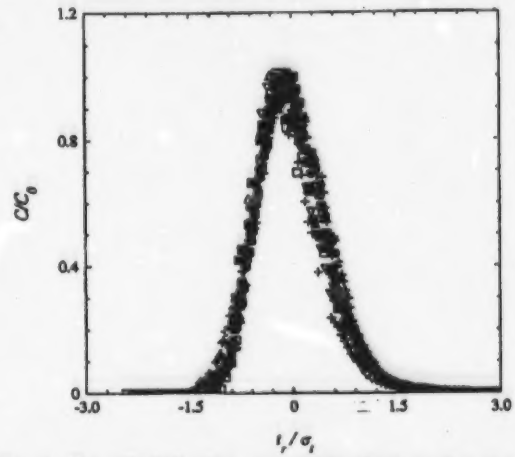

Fig. 2. The ensemble-mean concentration-time profiles for the cloud measured in various statistical ensembles at crosswind position $y_r = 0$. The ensemble-mean concentration, C, has been normalized by the ensemble-mean concentration, C_0, at the centroid ($C_0 \equiv C(y_r = 0, t_r = 0)$). The temporal profiles are plotted with respect to the normalized time, t_r/σ_t.

contaminant concentration is a random variable owing to the fact that the puff is dispersing in a turbulent atmospheric flow, one would be required to determine at minimum the mean and mean-square value (variance) to characterize the evolving concentration field. To this end, the ensemble-mean concentration, $C(y_r, t_r)$, is estimated from

$$C(y_r, t_r) \equiv \langle \chi_r(y_r, t_r) \rangle_n = \frac{1}{n} \sum_{j=1}^{n} \chi_r^{(j)}(y_r, t_r). \quad (8)$$

Similarly, the concentration variance $\sigma_c^2(y_r, t_r)$ is estimated from

$$\sigma_c^2(y_r, t_r) \equiv \langle \chi_r'^2(y_r, t_r) \rangle_n = \frac{1}{n} \sum_{j=1}^{n} [\chi_r^{(j)}(y_r, t_r) - C(y_r, t_r)]^2. \quad (9)$$

Fig. 1 displays the crosswind profiles of the ensemble-mean concentration $C(y_r, t_r)$ evaluated at $t_r = 0$. Each ensemble-mean concentration cross-section has been normalized by C_0, which is defined as the mean concentration value at the puff centroid (i.e. the mean concentration value evaluated at $(y_r, t_r) = (0, 0)$). Furthermore, the crosswind distance y_r from the mean puff centroid is normalized by the mean concentration puff dispersion, $\sigma_{G,y}$. The mean concentration puff dispersion was calculated using crosswind profile integration at $t_r = 0$, viz.

$$\sigma_{G,y} \equiv \left(\frac{\int y_r^2 C(y_r, t_r = 0)\, dy_r}{\int C(y_r, t_r = 0)\, dy_r} \right)^{1/2}. \quad (10a)$$

Although the instantaneous crosswind profiles of the puff concentration exhibited random variations in the concentration, the crosswind profiles of the ensemble-mean concentration are much more regular. The regularity of the ensemble-mean concentration lateral profiles suggests that the number of realizations in the various statistical ensembles was large enough to give a reliable statistical average. Interestingly, the form of $C(y_r, t_r = 0)/C_0$ for the various statistical ensembles is well approximated by a standard Gaussian function of $y_r/\sigma_{G,y}$. Fig. 2 exhibits the normalized ensemble-mean concentration-time profiles $C(y_r, t_r)/C_0$, evaluated at $y_r = 0$, as a function of the normalized time, t_r/σ_t. The mean "length" or duration of the puff was calculated by integration through the ensemble-mean concentration-time profile at $y_r = 0$, viz.

$$\sigma_t \equiv \left(\frac{\int t_r^2 C(y_r = 0, t_r)\, dt_r}{\int C(y_r = 0, t_r)\, dt_r} \right)^{1/2}. \qquad (10b)$$

The ensemble-mean concentration-time profiles exhibit a self-similar form. However, unlike the crosswind profiles, the time profiles deviate from a Gaussian shape. In particular, it was found that the leading edge of the mean concentration-time profiles rise more rapidly than the trailing edge, resulting in a shape that is non-symmetrical (viz., the curves appear to be skewed to the right). A closer inspection of this shape reveals that it exhibits a rapid Gaussian rise in the leading (front) part of the puff up to the puff center, followed by an elongated exponential fall in the trailing (back) part of the puff.

Similarly, the crosswind profiles of the concentration variance σ_c^2 at $t_r = 0$, when normalized by the concentration variance $\sigma_{c,0}^2$ at the puff centroid, assumed a Gaussian form when plotted against the normalized lateral distance, $y_r/\sigma_{Gc,y}$. Here, $\sigma_{Gc,y}$ is the crosswind standard deviation for the concentration variance lateral profile $\sigma_c^2(y_r, t_r = 0)$. Interestingly, it was found that the crosswind standard deviation of the ensemble-mean concentration profile is larger than that of the concentration variance profile by a factor of about 1.2 (viz., $\sigma_{G,y} \approx 1.2\sigma_{Gc,y}$). Also, the normalized concentration variance time profiles were found to possess a similar shape to that observed in the normalized ensemble-mean concentration-time profiles. However, it must be stressed that concentration variance time profiles appear to exhibit a faster rise and a subsequent faster descent from its peak value than the corresponding ensemble-mean concentration-time profiles. Furthermore, it was determined that the nondimensional half-life, $t_{r,1/2}^* \equiv t_{r,1/2}/\sigma_t$ (viz., the time taken for the normalized quantity to fall to one-half of its peak value), of the ensemble-mean concentration-time profile is roughly twice that of the corresponding concentration variance time profile. In summary, the crosswind cross-sections and the time profiles of the ensemble-mean concentration and concentration variance were found have self-preserving forms over the range of downwind fetches and atmospheric conditions covered by our experiments, but the profiles of the concentration variance tend to be narrower than those of the corresponding ensemble-mean concentration in both the y- and t-directions. This observation has important implications for the modelling of concentration fluctuations. In particular, the expedient modelling assumption that functional forms for the ensemble-mean concentration and concentration variance are exactly the same certainly appears to be flawed in the light of the current measurements.

Table 3
Summary of the mean cloud crosswind width and the cloud centroid values for the various statistical ensembles. Here, t is the travel time; $\sigma_{G,y}$ is the crosswind mean cloud width; C_0 is the value of the ensemble-mean concentration at the cloud centroid; and, $\sigma_{c,0}^2$ is the value of the concentration variance at the cloud centroid

Ensemble	t (s)	$\sigma_{G,y}$ (m)	C_0 (ppm)	$\sigma_{c,0}^2$ (ppm^2)
R01	34.7	5.45	33.02	1245
R02	34.3	9.86	37.83	1434
R03	39.1	6.40	62.90	1805
R04	85.3	8.69	3.16	10.02
R05	97.2	15.8	0.77	1.22
R06	175.2	26.7	1.99	11.42
R07	115.7	13.6	4.56	80.89
R08	87.4	12.3	12.74	112.4
R09	85.5	9.04	26.95	129.3
R10	116.5	8.38	18.68	82.03
R11	103.7	19.6	2.29	5.46
R12	113.9	28.1	3.62	5.08
R13	164.6	29.5	1.75	1.88
R14	203.5	25.0	4.21	11.59
R15	282.3	15.0	11.66	30.80
R16	170.5	30.3	1.58	1.37
R17	218.8	20.9	5.70	4.41

Next, we consider the downwind evolution of the puff growth and of the puff concentration moments at the centroid. The relevant variables used for studying the downwind variation of puff "size" and puff centroid concentration moments are summarized in Table 3. In order to study the variation of these quantities with travel time t from the source, it is necessary to combine a number of different statistical ensembles conducted under a variety of release and meteorological conditions. Hence, any variation will depend on the turbulence characteristics and the source strength as well as on t, with the result that appropriate normalizations of t and the puff size and concentration moments will need to be found if these quantities are to be compared at a range of travel times. Because the diffusion experiments considered in this study involve near ground-source instantaneous releases over relatively short downwind fetches, implying that the

diffusion occurred primarily in the atmospheric surface layer (constant stress layer), it is useful to apply surface-layer "similarity" theory or dimensional analysis in which physical insight is brought to bear to choose the proper characteristic variables or parameters. To this purpose, it is hypothesized that the downwind evolution of the puff size and puff centroid values of the concentration moments in the surface flux layer (as summarized in Table 3) can be ordered if they are non-dimensionalized by appropriate combinations of the primary variables that determine the characteristics of the surface layer and the source release; namely, u_*, the surface friction velocity that is indicative of the shear stress at the ground; L, the Monin–Obukhov length which can be interpreted as a stability parameter and is itself defined by the surface fluxes of heat and momentum; and Q, the source strength (release mass). Consequently, for any quantity, Φ, describing the dispersing puff and which varies with travel time, application of dimensional analysis with the primary variables enumerated above leads to a consideration of the relationship

$$\Phi = \Phi_* \mathcal{F}\left(\frac{u_* t}{|L|}\right), \tag{11}$$

where Φ_* is a combination of the primary variables that has the same dimensions as Φ. Here, $\mathcal{F}(\cdot)$ is a similarity function that relates the non-dimensional variable Φ/Φ_* to the non-dimensional travel time $u_* t/|L|$.

Fig. 3 shows a double-logarithmic plot of the normalized mean puff size, $\sigma_{G,y}/|L|$, versus non-dimensional travel time, $u_* t/|L|$. We found that the growth of the mean cloud can be well approximated by

$$\frac{\sigma_{G,y}}{|L|} = A_1 \left(\frac{u_* t}{|L|}\right)^n, \tag{12}$$

where A_1 was 0.71 ± 0.05 and the exponent n was 1.1 ± 0.05. For practical purposes, the mean puff growth over the regime of cloud development associated with our data can be simply approximated as follows,

$$\sigma_{G,y} = 0.71 u_* t. \tag{13}$$

Hence, over the range of travel times and meteorological conditions covered by our data, the lateral cloud size is seen to increase linearly (approximately or better) with t. This stage of cloud evolution corresponds to the turbulent-convective regime of development. The turbulent-convective regime is the central stage of cloud development where scales in the energy-containing range of the turbulence contribute to the cloud expansion. In this regime, growth of the cloud size is proportional to the travel time. It is expected that at still longer travel times, the rate of increase of the cloud size will decrease as the cloud development enters into the turbulent-diffusive regime. In this regime, the growth of the cloud size becomes proportional to the square root of the time.

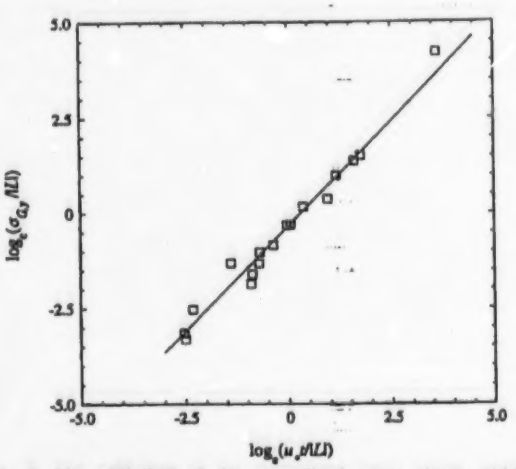

Fig. 3. The evolution of the normalized mean plume width, $\sigma_{G,y}/|L|$, with the normalized travel time, $u_* t/|L|$. The straight line is the curve $\sigma_{G,y}/|L| = 0.71(u_* t/|L|)^{1.1}$.

Fig. 4 shows how the non-dimensional cloud centroid ensemble-mean concentration, C_0/C_* ($C_* \equiv Q/|L|^3$), decreases as the non-dimensional mean cloud size, $\sigma_{G,y}/|L|$, increases. The decay of the cloud centroid mean concentration is well represented by

$$\frac{C_0}{C_*} = A_2 \left(\frac{\sigma_{G,y}}{|L|}\right)^m, \tag{14}$$

where A_2 was found to be 0.045 ± 0.009 and the exponent m to be -3.0 ± 0.1. Hence, in view of Eq. (13), it is seen that $C_0/C_* \sim (u_* t/|L|)^{-3}$.

The decrease of the non-dimensional cloud centroid concentration variance, $\sigma_{c,0}^2/\sigma_{c*}^2$ ($\sigma_{c*}^2 \equiv Q^2/|L|^6$), with non-dimensional mean cloud size, $\sigma_{G,y}/|L|$, is displayed in Fig. 5. It was found that this decrease can be approximated by the power-law relationship

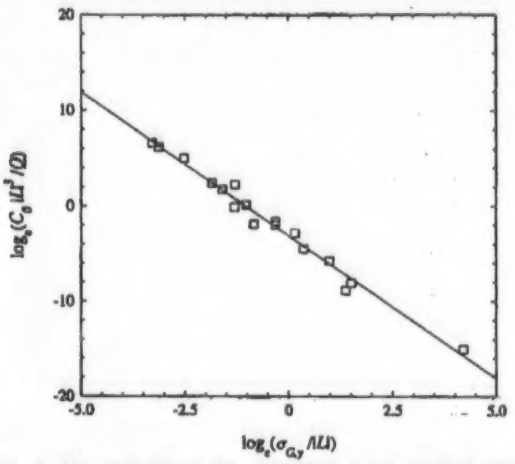

Fig. 4. The variation of the normalized cloud centriod ensemble-mean concentration, C_0/C_* ($C_* \equiv Q/|L|^3$), plotted against the normalized lateral cloud width, $\sigma_{G,y}/|L|$. The straight line is the curve $C_0/C_* = 0.045(\sigma_{G,y}/|L|)^{-3}$.

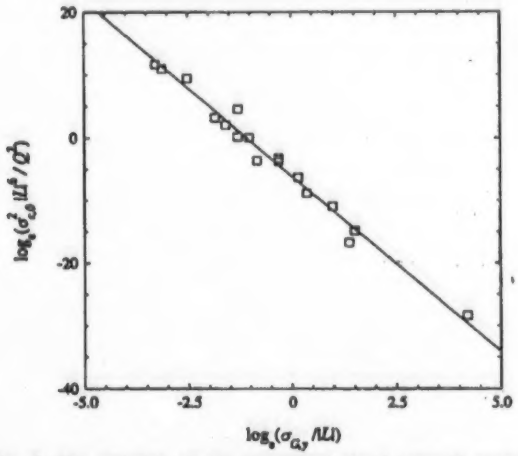

Fig. 5. The variation of the normalized cloud centroid concentration variance, $\sigma_{c,0}^2/\sigma_{c*}^2$ ($\sigma_{c*}^2 \equiv Q^2/|L|^6$), plotted against the normalized lateral cloud width, $\sigma_{G,y}/|L|$. The straight line is the curve $\sigma_{c,0}^2/\sigma_{c*}^2 = 0.0022(\sigma_{G,y}/|L|)^{-5.6}$.

$$\frac{\sigma_{c,0}^2}{\sigma_{c*}^2} = A_3\left(\frac{\sigma_{G,y}}{|L|}\right)^p, \tag{15}$$

where $A_3 = 0.0022 \pm 0.0004$ and $p = -5.6 \pm 0.2$. The results embodied in Figs. 4 and 5 9or, equivalently, in the relationships summarized in Eqs. (13)–(15)) imply that the cloud centroid fluctuation intensity, $\sigma_{c,0}/C_0$, is a very weak function of travel time t since it is seen that the concentration standard deviation $\sigma_{c,0}$ falls off with travel time t roughly as fast as the mean concentration C_0. In particular, it was found that $\sigma_{c,0}/C_0$ varies like $(u_*t/|L|)^r$, where $r = 0.2 \pm 0.2$. Hence, the fluctuation intensity, which gives a measure of the fluctuations within the instantaneous cloud, appears to increase like $t^{0.2}$ in the turbulent-convective regime of cloud development. However, it should be stressed that this putative rate of increase in the centroid fluctuation intensity is very small and, certainly, the alternative interpretation that the fluctuation intensity achieves a near-constant non-zero value within the turbulent-convective regime cannot be ruled out given the experimental scatter in our data.

The results of our experiments can be compared with Lagrangian similarity modelling of the diffusion of a puff in the constant stress layer. Lagrangian similarity predictions of mean concentrations in a dispersing cloud are based on the sound theoretical work of Batchelor [15] and Chatwin [16], wherein the important variables and governing parameters in the problem are chosen and normalized so as to provide simple dimensionless relations among them that can be used to predict the location of the center-of-mass and spatial extent of the dispersing cloud provided that it remains within the constant stress layer. The modelling of the contaminant cloud diffusion can be decomposed into the determination of three basic quantities; namely, the location, size, and state in the cloud. The Lagrangian similarity analysis predicts that the center-of-mass (location) $(\overline{x}, \overline{y}, \overline{z})$ (in the alongwind, crosswind, and vertical directions) of a contaminant cloud released from an instantaneous source near the ground into a neutrally stratified constant stress layer is given by [16]

$$\overline{x} = \frac{u_*t}{\kappa}\left[\log_e\left(\frac{0.56\kappa u_* t}{z_0}\right) - 1\right], \tag{16a}$$

$$\overline{y} = 0, \tag{16b}$$

$$\overline{z} = \kappa u_* t. \tag{16c}$$

The standard deviations σ_x, σ_y, and σ_z for the spatial extent (size) of the cloud is given by [16]

$$\sigma_x(t) = \frac{0.803u_*t}{\kappa}, \tag{17a}$$

$$\sigma_y(t) = \sqrt{2}\kappa u_* t, \tag{17b}$$

$$\sigma_z(t) = \kappa u_* t. \tag{17c}$$

Finally, if we assume that the mean cloud concentration (state) can be represented by a trivariate Gaussian form with centroid $(\bar{x}, \bar{y}, \bar{z})$ and standard deviations $\sigma_x, \sigma_y, \sigma_z$ in the alongwind, crosswind, and vertical directions, the maximum value for the Gaussian distribution occurs at its centroid and is given by

$$C_0 = \frac{Q}{(2\pi)^{3/2}\sigma_x\sigma_y\sigma_z}. \tag{18}$$

Hence, the maximum mean concentration value at the centroid is estimated by considering the total release mass Q to be confined to a volume $(2\pi)^{3/2}\sigma_x\sigma_y\sigma_z$.

While our data did not enable us to determine $\bar{x}$ and $\bar{z}$ as a function of travel time t, the measured lateral growth of the cloud can be compared directly to the Lagrangian similarity predictions. To this end, it is noted that Eq. (17b) predicts that $\sigma_y(t) = 0.57u_*t$, which agrees quite well with the observed relationship summarized in Eq. (13). Furthermore, the ensemble-mean concentration at the center-of-mass is predicted by Lagrangian similarity analysis to vary with travel time t as follows (cf. Eqs. (17) and (18)),

$$C_0 = \frac{A'Q}{(u_*t)^3}, \tag{19}$$

where $A' = 0.14$. Using the measured relationships between C_0 and $\sigma_{G,y}$ and between $\tau_{G,y}$ and u_*t summarized in Eqs. (14) and (13), respectively, it was found that the measured C_0 varies with u_*t as follows,

$$C_0/C_* = 0.13\left(\frac{u_*t}{|L|}\right)^{-3}. \tag{20}$$

Hence, provided an account is made for diabatic effects, the decay of the cloud centroid mean concentration with travel time appears to be well represented by the Lagrangian similarity predictions (cf. Eqs. (19) and (20)). However, it should be emphasized that our observed values of C_0 correspond to the centroid in the (y, t) plane at the detector height z_d, whereas the predicted values of C_0 were obtained at the true center-of-mass of the cloud. However, the favorable comparison between the results of Eqs. (19) and (20) would suggest that the value of the ensemble-mean concentration at the center-of-mass (whose vertical position is at $\bar{z}$) is not that different from that measured at the detector height z_d. This observation appears to be consistent with the Lagrangian similarity prediction that there is a growing region in the dispersing cloud for which the distribution of pollutant is independent of height [16].

The downwind variation of the cloud centroid concentration variance can be investigated by consideration of the transport equation for the scalar variance,

$$\frac{\partial\sigma_c^2}{\partial t} = -U_i\frac{\partial\sigma_c^2}{\partial x_i} - 2\langle u_i'\chi'\rangle\frac{\partial C}{\partial x_i} - \frac{\partial}{\partial x_i}\langle u_i'\chi'^2\rangle - 2\epsilon_c, \tag{21}$$

where the summation convention, whereby repeated indices are summed, has been assumed. Here, $U_i \equiv \langle u_i\rangle$ and $u_i' \equiv u_i - U_i$ are the mean velocity and velocity fluctuations in the ith coordinate direction. Furthermore, $\langle\cdot\rangle$ denotes the ensemble averaging operation, and $\epsilon_c \equiv D\langle(\partial\chi'/\partial x_i)^2\rangle$ is dissipation rate for concentration fluctuations (D is the molecular diffusion coefficient). In Eq. (21), the term on the left represents the local storage of concentration variance, whereas the terms on the right represent advection, production by flux-gradient interactions with the mean concentration field, turbulent transport, and dissipation of concentration variance. The turbulent transport term is in divergence form; hence, this term can be eliminated by a spatial integration since it has zero integral over all space and, in essence, simply represents the transfer of σ_c^2 from place to place in the cloud.

If we assume that $C_0^2 \sim t^{-\mu}$ and $\sigma_{c,0}^2 \sim t^{-\nu}$, then it is seen that the storage term scales varies as $t^{-\nu-1}$, whereas the advection term varies as $t^{-\nu-1}$ on using the fact that $x \sim u_*t$. Let us assume that the concentration flux $\langle u_i'\chi'\rangle$ can be approximated using a gradient-diffusion postulate of the form

$$\langle u_i'\chi'\rangle = -K_E\frac{\partial C}{\partial x_i}, \tag{22}$$

where K_E is an eddy diffusivity. Then, by an analogy with molecular diffusion, K_E may be defined by the relationship

$$K_E \equiv \frac{1}{2}\frac{d\sigma_{G,y}^2}{dt}. \tag{23}$$

Eq. (22) implies that the production term in Eq. (21) is of order $K_E C_0^2/\sigma_{G,y}^2$. Since Eqs. (23) and (13) further imply that $K_E \sim t$ in the turbulent-convective

regime of development, it follows then that the production term varies as $t^{-\mu-1}$. Finally, if we parametrize the dissipation as $\epsilon_c \sim \sigma_{c,0}^2/\tau_c$ where τ_c is a suitable dissipation time scale, and if we assume that $\tau_c \sim \sigma_{G,y} \sim t$, then we find that the dissipation term in Eq. (21) varies as $t^{-\nu-1}$. Now, comparing the orders-of-magnitude of all the terms in Eq. (21), it follows that the only possible balance must be a balance between the production and dissipation terms, from which it can be concluded that $\mu = \nu$. Hence, with an eddy diffusivity and dissipation time scale that increase linearly with travel time t in the turbulent-convective regime, the balance between production and dissipation implies that the ensemble-mean concentration and concentration standard deviation at the cloud centroid decay at the same rate with increasing t. Furthermore, this implies that the fluctuation intensity, $\sigma_{c,0}/C_0$, must remain constant with travel time within the turbulent-convective regime of cloud development. This simple scaling analysis produces results that accord well with our observations of cloud dispersion.

The production-dissipation balance is a manifestation of the balance between the simultaneous effects of turbulent stirring (i.e. strain-induced stretching of the material surface) and molecular mixing (i.e. molecular diffusion of contaminant across the material surface). Indeed, cloud contaminant elements are simultaneously distended, folded, and distorted by the turbulent convective motions into ever thinning and convoluted strands and ribbons. This action maintains the ever increasing streakiness of the scalar, and is the source of production of the concentration fluctuations. However, the dramatic increase in the concentration gradients arising from the thinning of the contaminant elements due to turbulent convective stirring must eventually be balanced by the thickening due to molecular diffusion, whose dissipation effects on the concentration fluctuations are enhanced by the increasing concentration gradients. Hence, the production-dissipation balance simply reflects the balance between the turbulent stirring and molecular mixing in the cloud. In the turbulent-convective regime of cloud development, the rate of decrease of the ensemble-mean concentration and concentration standard deviation both scale as t^{-p} ($p \approx 3$). Furthermore, the lateral cloud size $\sigma_{G,y} \sim t$ in this regime of development, which implies that the effective diffusivity $K_E(t)$ governing the dispersion process scales as t ($K_E(t) \sim \mathrm{d}\sigma_{G,y}^2/\mathrm{d}t$), as does the dissipation time scale τ_c. In this regime, the size of the effective eddies responsible for the cloud growth embrace those in the energy-containing range in the turbulence spectrum in which the growth of $\sigma_{G,y}$ becomes proportional to the travel time itself. Here, the downwind variation of the concentration fluctuation intensity is a constant, implying that the turbulent stirring that is responsible for the development of structure of ever-increasing scale in the cloud is exactly balanced by the molecular mixing that is responsible for the smoothing of the fine-scale structure in the cloud.

At shorter travel times before the transition into the turbulent-convective regime of cloud development, the eddies responsible for expanding the cloud by entraining clean air (e.g., eddies of a similar scale to the instantaneous size of the cloud) embrace scales in the inertial subrange of turbulence. The turbulence spectral density increases for scales within the inertial subrange as the cloud grows, and the rate of growth of the cloud must then depend only on the rate of dissipation, ϵ, of turbulence kinetic energy and the travel time. Dimensional analysis then demands that $\sigma_{G,y}^2 \sim \epsilon t^3$ within this regime of cloud development. This stage of development is the inertial-convective regime wherein the cloud size increases as $t^{3/2}$. Using arguments similar to those applied above for the turbulent-convective regime, it can be seen that the production term of Eq. (21) varies as $t^{-\mu-1}$ in the inertial-convective regime since $K_E \sim t^2$. Furthermore, the molecular dissipation term of Eq. (21) varies as $t^{-\nu-3/2}$, assuming that $\tau_c \sim \sigma_{G,y} \sim t^{3/2}$. Hence, the balance between production (gain) and dissipation (loss) in the inertial-convective regime implies that $\mu = \nu + 1/2$. This, in turn, implies that the fluctuation intensity, $\sigma_{c,0}/C_0$, increases as $t^{1/4}$. The increase of the fluctuation intensity with travel time within the inertial-convective regime suggests that the effects of turbulent stirring are greater than those of molecular mixing, producing an increase in the small-scale structure in the cloud.

Finally, at longer travel times occurring after the end of the turbulent-convective regime of cloud development (e.g., at travel times much greater than those covered by our experiments), the rate of growth of $\sigma_{G,y}^2$ will decrease from that in the turbulent-convective regime and become a constant as the cloud enters into the turbulent-diffusive regime of development. In this

regime, $\sigma_{G,y} \sim t^{1/2}$ [17]. The production term of Eq. (21) must then vary as $t^{-\mu-1}$ in the turbulent-diffusive regime because $\sigma_{G,y} \sim t^{1/2}$ implies that $K_E(t)$ is a constant. Furthermore, the dissipation term of Eq. (21) must vary as $t^{-\nu-1/2}$, if we again assume that $\tau_c \sim \sigma_{G,y} \sim t^{1/2}$. Again, the budget of σ_c^2 is basically a balance between production (gain) and dissipation (loss) in the dispersing cloud. In the turbulent-diffusive regime, this balance implies that $\mu = \nu - 1/2$. This, in turn, implies that the fluctuation intensity, $\sigma_{c,0}/C_0$, in the cloud must decrease with travel time in the turbulent-diffusive regime as $t^{-1/4}$. This suggests that the effects of molecular mixing are stronger than those of turbulent stirring in the turbulent-diffusive regime, and that with continued mixing and homogenization of the in-cloud structure, the fluctuation intensity decreases toward zero in the final, fully mixed asymptotic state. The implicit assumption in this prediction is that the size of the cloud in this regime embraces eddies in the energy-containing range of the turbulence spectrum over increasing scales whereby the spectral energy decreases as the cloud grows. Naturally, in the atmosphere, where large velocity fluctuation scales arising from mesoscale motion systems can be present, the turbulent-diffusive regime of cloud development may not persist to the asymptotic state of cloud development.

List of symbols

C ensemble-mean concentration
C_0 ensemble-mean concentration at cloud centroid
C_* ensemble-mean concentration scale ($\equiv Q/|L|^3$)
K_E eddy diffusivity
n number of puffs in an ensemble
L Monin–Obukhov length
Q source mass
t travel time (time elapsed since pollutant material left its source)
$t_C^{(j)}$ time centroid location of the jth puff in an ensemble
t_r time referenced to time centroid ($\equiv t - t_C^{(j)}$)
y crosswind distance in absolute coordinates
$y_C^{(j)}$ crosswind centroid location of the jth puff in an ensemble
y_r crosswind distance referenced to crosswind centroid ($\equiv y - y_C^{(j)}$)
u_* friction velocity
U mean wind speed
U_T global mean transport speed
$U_T^{(j)}$ local mean transport speed of the jth puff in an ensemble
ϵ dissipation rate of turbulence kinetic energy
ϵ_c dissipation rate of concentration fluctuations
κ Von Karman's constant (≈ 0.4)
σ_c^2 concentration variance
$\sigma_{c,0}^2$ concentration variance at cloud centroid
σ_{c*}^2 concentration variance scale ($\equiv Q^2/|L|^6$)
$\sigma_{G,y}$ dispersion of ensemble-mean concentration crosswind profile
$\sigma_{Gc,y}$ dispersion of concentration variance crosswind profile
σ_t dispersion of ensemble-mean concentration-time profile
σ_u standard deviation of velocity fluctuations in alongwind direction
σ_v standard deviation of velocity fluctuations in crosswind direction
σ_w standard deviation of velocity fluctuations in vertical direction
τ_c concentration dissipation time scale
χ instantaneous concentration in absolute coordinates
χ_r instantaneous concentration in relative coordinates

References

[1] S.R. Hanna, Boundary-Layer Meteorol. 29 (1984) 361.
[2] B.L. Sawford, C.C. Frost, T.C. Allan, Boundary-Layer Meteorol. 31 (1985) 249.
[3] B.L. Sawford, Boundary-Layer Meteorol. 38 (1987) 209.
[4] N. Dinar, H. Kaplan, M. Kleiman, Boundary-Layer Meteorol. 45 (1988) 157.
[5] S.R. Hanna, E.M. Insley, Boundary-Layer Meteorol. 47 (1989) 131.
[6] H. Peterson, B. Lamb, D. Stock, J. Appl. Meteorol. 29 (1990) 1284.
[7] K.R. Myine, P.J. Mason, Q.J.R. Meteorol. Soc. 117 (1991) 177.

[8] K.R. Mylne, Boundary-Layer Meteorol. 60 (1992) 15.
[9] E. Yee, R. Chan, P.R. Kosteniuk, G.M. Chandler, C.A. Biltoft, J.F. Bowers, J. Appl. Meteorol. 33 (1994) 996.
[10] E. Yee, R. Chan, P.R. Kosteniuk, G.M. Chandler, C.A. Biltoft, J.F. Bowers, Boundary-Layer Meteorol. 76 (1995) 41.
[11] F.N. Frankiel, I. Katz, J. Meteorol. 13 (1956) 388.
[12] U. Högström, Tellus 16 (1964) 205.
[13] P.W. Nickola, J. Appl. Meteorol. 10 (1971) 962.
[14] P.J. Drivas, F.H. Shair, Atmos. Environ. 8 (1974) 475.
[15] G.K. Batchelor, Arch. Mech. Stosow. 3 (1964) 661.
[16] P.C. Chatwin, Q.J.R. Meteorol. Soc. 94 (1968) 401.
[17] G.I. Taylor, Proc. London Math. Soc. Ser. 2 20 (1921) 196.

#509354

CONTENTS ALERT™

A CURRENT AWARENESS SERVICE
FREE OF CHARGE
VIA ELECTRONIC MAIL

FOR SCIENTISTS WORKING IN THE FIELD OF SURFACES, INTERFACES AND THIN FILMS

FOR SCIENTISTS WORKING IN THE FIELD OF MATHEMATICAL & THEORETICAL METHODS IN PHYSICS

As the number of scientific publications grows daily it becomes increasingly important to trace the most interesting publications in a way that costs as little time as possible.

Elsevier Science Publishers now provides CONTENTS-Alert, ***a free electronic service*** that can assist you in carrying out time-saving searches on a regular, two-weekly basis.

CONTENTS-Alert is a current awareness service which delivers, through e-mail, the tables of contents of a selected group of journals. Not only will you receive these tables of contents ***before or upon publication*** of the journals but you can also browse through these tables of contents ***at your own terminal***, in your own time. A survey carried out among researchers using CONTENTS-Alert has shown that this free service is very convenient and time-effective.

We offer two versions of CONTENTS-Alert each covering a specific field. One version of CONTENTS-Alert includes journals on Surfaces, Interfaces and Thin Films, and one includes journals on Mathematical and Theoretical Methods in Physics.

Journals covering the field of Surfaces, Interfaces and Thin Films
Applied Surface Science Chemical Physics Letters Materials Science and Engineering: R: Reports Nuclear Instruments and Methods in Physics Research: Section B Surface Science (including Surface Science Letters) Surface Science Reports Thin Solid Films Vacuum
Our e-mail for this version is: RFC-822: C-ALERT@ELSEVIER.NL X.400: C=NL;A=400NET;P=SURF;O=ELSEVIER;S=C-ALERT

Journals covering the field of Mathematical and Theoretical Methods in Physics
Computer Physics Communications Journal of Geometry and Physics Nuclear Physics B Physica A Physica D Physics Letters A Physics Letters B Physics Reports Wave Motion
Our e-mail for this version is: RFC-822: C-ALERT.MATHPHYS@ELSEVIER.NL X.400: C=NL;A=400NET;P=SURF;O=ELSEVIER; S=MATHPHYS; G=C-ALERT

Subscribe now to this *free pre-publication service* and find out how useful CONTENTS-Alert really is. Just send your full address to the e-mail number quoted above that corresponds with the CONTENTS-Alert version you wish to receive, or send it by post and we will make sure you will receive CONTENTS-Alert every two weeks.
Please allow three weeks processing time for your free subscription.

Yes, please add my name to the circulation list of **CONTENTS-Alert.**

Version: ☐ Surfaces, Interfaces and Thin Films
☐ Mathematical and Theoretical Methods in Physics

Return to:

ELSEVIER SCIENCE PUBLISHERS B.V.,
Att: Mr. M. Stavenga,
P.O. BOX 103, 1000 AC Amsterdam, The Netherlands
Fax 31 20 5862580

Name _____
Initials _____ Title _____ ☐ Male ☐ Female
Institute _____
Department _____
Street/ PO Box _____
City _____
Country _____
Tel: _____ Fax: _____
E-mail _____